Electron emission characterization of Mg photocathode grown by pulsed laser deposition within an *S*-band rf gun

L. Cultrera,[1] G. Gatti,[1] P. Miglietta,[2] F. Tazzioli,[1] A. Perrone,[2] J. T. Moody,[3] and P. Musumeci[3]
[1]*National Institute of Nuclear Physics, National Laboratories of Frascati, Via E. Fermi 40, Frascati, Italy*
[2]*National Institute of Nuclear Physics and Physics Department, University of Salento, Via per Arnesano, Lecce, Italy*
[3]*UCLA, Department of Physics and Astronomy, Los Angeles, California 90095, USA*
(Received 13 October 2008; published 30 April 2009)

Pulsed laser deposition (PLD) has been proposed several years ago as a suitable technique to deposit a pure Mg film over a radio frequency (rf) gun Cu backflange in order to obtain a high efficiency photocathode surface for the generation of high brightness electron beams. In this paper we report preliminary experimental results on the emission properties of a PLD grown Mg film within the high electric field gradients of a rf gun showing the effects of the rf conditioning process on the cathode surface. Even though a laser cleaning process should be performed on the sample surface in order to remove contaminated layers, the results presented here are very promising for the realization of a final Mg-based photocathode.

DOI: 10.1103/PhysRevSTAB.12.043502 PACS numbers: 79.60.−i, 29.25.Bx, 29.27.−a, 81.15.−z

I. INTRODUCTION

Electron injectors for advanced projects such as fourth generation x-ray FEL sources [1], and for future linear colliders [2], are most commonly based on laser excited photocathodes located in high field guns. The main requirements on the cathodes are high quantum efficiency, promptness of response, emission uniformity over the irradiated surface, and stability (lifetime). Metals have fast response times, typically in the tens of femtoseconds or shorter range and they are rugged in handling. Although a very large number of metallic photocathodes have been prepared and extensively studied [3], only a few of them could find significant technological applications. Mg-based photocathodes have been the most studied due to their respectable quantum efficiency [4].

Sputtered Mg films have already been tested in rf guns. However, when tested in the very high electric fields of a rf gun, the sputtered Mg films have been found to be seriously damaged by discharges during rf conditioning [5]. This has been ascribed to the poor quality of the film, especially regarding uniformity and adhesion to the Cu substrate.

Previous reports on Mg films grown by pulsed laser deposition (PLD) showed promising results, in particular, with respect to uniformity of emission, quantum yield, and adhesion to the substrate [6]. Progress in the basic understanding of the influence of the gas absorption on the quantum efficiency of such cathodes and on the procedure for performing the laser cleaning treatments required to improve their photoemissive properties has also been reported [7].

One aspect that deserves further investigation is connected with the behavior of the Mg film based photocathode during its operation in a real rf gun. Here the films should withstand electric field gradients exceeding 100 MV/m and survive the conditioning process of the microwave cavities. Typically during the conditioning process, hundreds of electrical discharges take place on the inner surface of the cavities. In order to be suitable to operate in an rf gun, the Mg film based photocathode should not be destroyed during this process.

The aim of this paper is to describe our first experimental experience on the conditioning process and operation of a photocathode based on PLD grown Mg film.

II. EXPERIMENTAL APPARATUS

A. Cathode preparation

The PLD apparatus used to deposit thin films is shown in Fig. 1. The deposition of magnesium film was achieved using a 308 nm wavelength pulsed laser beam produced by

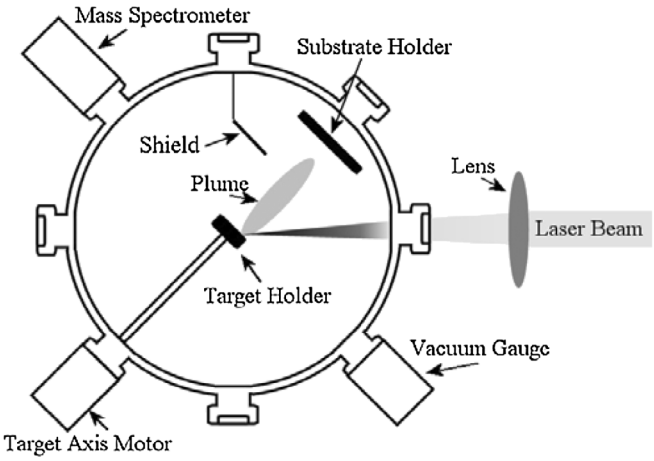

FIG. 1. Schematics of the pulsed laser deposition apparatus.

an XeCl* excimer laser ($\tau = 30$ ns). The laser was focused on a pure disk of magnesium (99.9%) rotating at a frequency of 1 Hz. The laser beam was incident on the target surface at an angle of 45°. The ablated material was collected on Cu backflange suitable to be inserted into the 1.6 cell UCLA/SLAC/BNL rf gun [8].

In order to remove the contaminants due to the machining processes and the oxide layers, the Cu polished flange has been cleaned in an ultrasonic bath of acetone for 30 minutes and in an ultrasonic bath of citric acid (0.05 mol/L) for 30 minutes. At the end of each bath with solvent, the substrate has been rinsed with ultrasonic bath in demineralized water for 30 minutes. The cleaning procedure in the ultrasonic bath has been performed at room temperature. At the end of the last bath, the substrate has been dried in an oven at 100°C for 10 minutes and readily inserted into the deposition chamber. The target-substrate distance was set 5.5 cm and the laser fluence was set at 10 J/cm^2. The PLD system was evacuated at a base pressure of about 5×10^{-6} Pa by a turbomolecular pump. In order to clean the target surface, a preirradiation treatment was applied with 5000 laser pulses. During this stage, the Cu substrate was shielded from the ablated material to prevent impurities contamination.

During deposition, a mask having a 1 cm diameter hole was used to restrict the Mg coated area only to a region around the geometrical center of the substrate. The deposition was carried out with 30 000 laser pulses. Under similar experimental conditions, the thickness of the Mg film was measured to be about 500 nm [9]. The mass spectra of the residual gases revealed that during the deposition process the most abundant chemical species in the deposition vacuum chamber were molecular nitrogen, water vapor, and molecular oxygen. Their partial pressures were respectively 4.5×10^{-6} Pa, 3.5×10^{-7} Pa, and 1.5×10^{-7} Pa.

FIG. 2. (Color) Picture of the Cu backflange. At the center is clearly visible the Mg film.

The morphology and the oxidation level of the cathode were investigated after the removal from the rf gun by scanning electron microscopy (SEM) and by energy dispersive x ray (EDX) with the aid of a SEM JEOL 6480LV microscope. A picture of the cathode flange with the Mg film is shown in Fig. 2.

B. Cathode installation and rf conditioning

After the deposition in the Physics Department of University of Salento, the cathode was shipped for installation in the rf gun at the UCLA PEGASUS photoinjector laboratory. The beam line used for these experiments, displayed in Fig. 3, is composed by a standard SLAC-UCLA-BNL 1.6 cell S-band rf gun, a focusing solenoid, a fluorescent screen for beam position monitoring, and a Faraday cup (FC).

Since no controlled gas environment was used during transportation, the Mg surface was expected to be polluted. The formation of the oxide layer over Mg, when exposed to air, has been proven by samples previously tested in a low electric field environment [7]. During the installation of the cathode, the gun was tuned through the standard capacitive backflange deformation [10]. The conditioning process took about 24 hours yielding a nearly arc-free operation of the rf gun at 100 MV/m peak field. The vacuum of the rf gun during operation ranges in the 10^{-7} Pa level.

C. Laser system

A Ti:sapphire laser system from Coherent Inc. generates pulses having 40 fs FWHM at 800 nm, as measured with a single shot autocorrelator [11]. After frequency tripling in thin crystals (300 μm for second harmonic and 150 μm for third harmonic generation) and thin lens-based optical transport to the cathode, the UV laser pulse is ~35 fs rms. The pulse-to-pulse energy fluctuations for the system are less than 1% rms, with good mode quality ($M^2 < 1.35$).

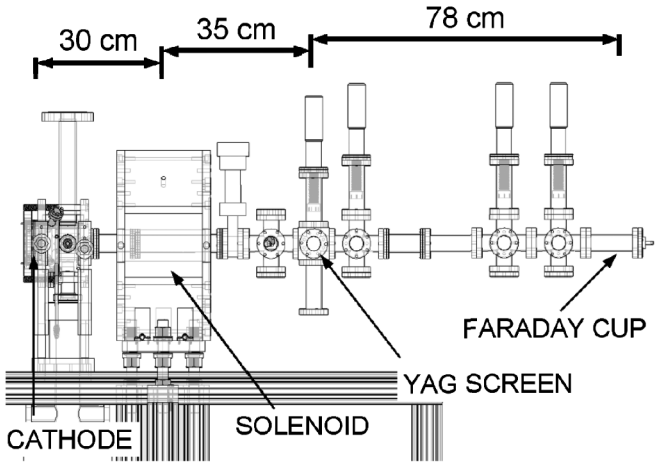

FIG. 3. Schematics of the PEGASUS rf-gun beam line.

III. EXPERIMENTAL RESULTS

A. Quantum efficiency

Figure 4 shows the charge collected by the Faraday cup (FC) as functions of the injection phase that is the time of arrival of the laser pulse with respect to rf wave inside the gun cavity. For these measurements, the focusing solenoid field was set at 1.15 kGs and the laser energy per pulse was about 2 μJ.

The emission curve of the cathode, reported in Fig. 5, was obtained by correlating the FC charge readout with the input laser energy sampled with a 1% beam splitter before the laser enters the vacuum chamber. For this measurement, the injection phase of the laser beam was set at 25°.

The emission curve shows a nonlinear behavior, evidence of oxidation of the Mg cathode surface.

In order to analyze both the collected charge vs launch phase and collected charge vs laser energy data, a numerical model of the emission process of the cathode in the presence of high electric fields has been implemented. The model takes account of both one- and two-photon electron emission, of image charge at the cathode surface, and of the spatiotemporal laser energy distribution.

Assuming the laser temporal distribution to be Gaussian with a σ_t of ~35 fs and its spatial distribution to be a Gaussian truncated at $0.8\sigma_r$ with a σ_r of ~700 μm, the optical power density can be expressed as

$$P_{\text{laser}}(t, r) = I_0\left[\frac{1}{2\pi\sigma_r^2}\exp\left(-\frac{r^2}{2\sigma_r^2}\right)\right] \times\left[\frac{1}{\sqrt{2\pi\sigma_t^2}}\exp\left(-\frac{t^2}{2\sigma_t^2}\right)\right], \quad (1)$$

where I_0 is the maximum value of laser intensity.

By integration of the P_{laser} between t and $t + dt$ and between r and $r + dr$, it is possible to determine the quantity of the laser energy deposited on the cathode surface during the time interval between t and $t + dt$ and within the annulus having internal radius r and external radius $r + dr$ as shown in the following:

$$I(t, dt, r, dr) = I_0\left[\int_r^{r+dr}\frac{1}{2\pi\sigma_r^2}\exp\left(-\frac{\bar{r}^2}{2\sigma_r^2}\right)d\bar{r}\right] \times\left[\int_t^{t+dt}\frac{1}{\sqrt{2\pi\sigma_t^2}}\exp\left(-\frac{\bar{t}^2}{2\sigma_t^2}\right)d\bar{t}\right]. \quad (2)$$

Knowing the laser intensity distribution, the electron current density emitted from the cathode can be evaluated taking in account one- and two-photon emission processes and the lowering of the work function induced by the Schottky effect due to the field at the cathode surface. Following the generalized Fowler-Dubridge theory on multiphoton emission stands [12],

$$\frac{d\sigma(t, r, dr)}{dt} = \sum_n a_n\left(\frac{e}{h\nu}\right)^n A\left(\frac{I(t, dt, r, dr)}{2\pi r dr dt}\right)^n \times (1 - R)^n T^2 \times F\left(\frac{n\cdot h\nu - \phi + \alpha\sqrt{\beta_{\text{ph}}E(t, r, dr)}}{kT}\right), \quad (3)$$

where a_n is an empirical parameter linked to the probability for the n-photon emission, A is the Richardson constant, e is the electron charge, $(1 - R)^n$ is the nonlinear bulk absorption coefficient, T is the sample temperature, F is the Fowler function, $h\nu$ is the photon energy, φ is the work function, $\alpha = 3.795 \times 10^{-5}$ is the fine structure constant in MKS units, β_{ph} is the field enhancement factor for the photoemission process, and $E(t, r, dr)$ is the electric field at the cathode. The latter is the sum of two contributions, the rf external field and the space charge field at the cathode surface:

$$E(t, r, dr) = E_0\sin(\varpi t) - \frac{1}{\varepsilon_0}\int_0^{t+dt}\frac{d\sigma(t, r, dr)}{d\bar{t}}d\bar{t}, \quad (4)$$

where ε_0 is the dielectric constant of vacuum, ω is the radian frequency of the rf , and E_0 is the amplitude of the electric field in the gun cavities. The total charge emitted can be calculated integrating the electron current density over space and time. A fit to the data using a simple ordinary least square minimization algorithm yields estimates of the values for $a1$, $a2$, β_{ph}, and φ.

In order to take into account the electron transport inside the rf gun, the emitted charge has been multiplied by a transport factor function having a value equal to 1 for launch phase ranging from 0° to 90° and equal to 0 otherwise. This assumption largely underestimates the amount of charge collected on the Faraday cup for injection phases higher than 90° (Fig. 4).

By using this algorithm, we were able to obtain good fits for both the collected charge vs launch phase and collected charge vs laser energy as reported in Figs. 4 and 5, respec-

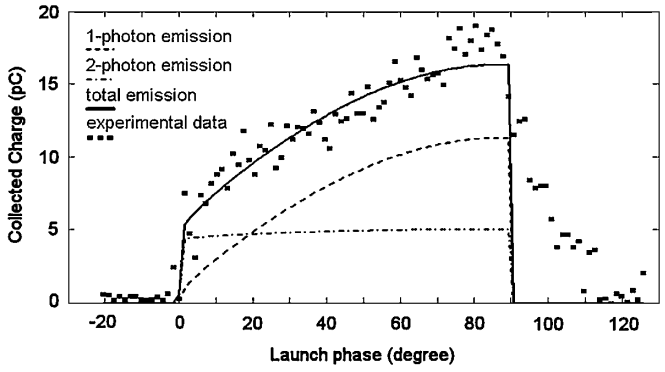

FIG. 4. Electron bunch charge vs launch phase: in the graph are reported the experimental data, and the emitted charge simulated by considering both one and two photoemission processes.

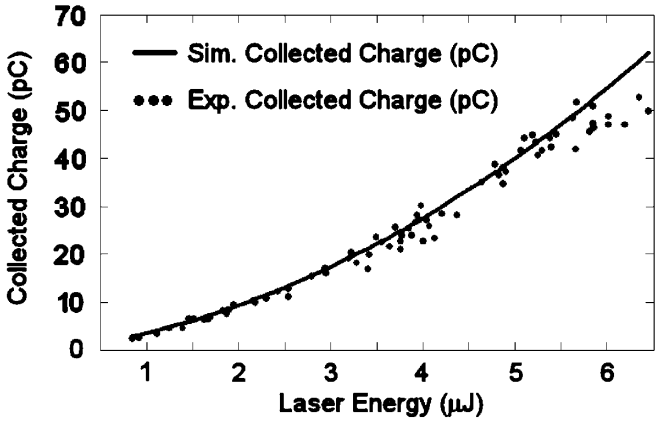

FIG. 5. Emission curve characteristic of this Mg film sample. The nonlinear correlation between bunch charge and laser energy due to the non-negligible contribution of the two-photon electron emission process is evident.

tively. The parameters that gave the best fit to the experimental data are reported in Table I.

The process of laser cleaning is expected to significantly improve the cathode electron yield for one-photon emission thus decreasing both the laser power density necessary to extract the desired given amount of charge and the quantity of electrons emitted by two-photon processes [7]. Recently published results on a photoemission experiment performed in low DC electric field showed that the highest quantum efficiency values of Mg (up to 10^{-3} level) may be achieved only after the removal of surface contaminated layers. In those experiments, emission curves obtained illuminating with a 4th harmonic of a Nd:YAG laser ($\lambda = 266$ nm, $\tau = 30$ ps) Mg samples grown by PLD in similar conditions and before any surface laser cleaning treatment show both linear and nonlinear behavior. This indicates that the emission process may be achieved through a one-photon absorption but also with a remarkable contribution given by two-photon absorption, as shown in Refs. [6,7] depending on the surface work function of the oxidized sample. X-ray diffraction spectra of Mg samples grown by PLD in conditions similar to those used on these experiments do not exhibit any dominant peak characteristic of MgO crystalline structure revealing that, if any oxide is formed at the sample surface, it has an amorphous structure.

MgO presents different values of work function depending on its crystallographic orientation. Work function values range between 4.22 eV for MgO (111) and 5.07 eV for MgO (220) orientation [7]. It looks reasonable to assume that amorphous MgO has a work function value that, averaged over the laser irradiated area, is close to the found value of 4.6 eV. The illumination of the cathode with photons at 4.67 eV could result then on a different contribution ratio between one- and two-photon adsorption processes depending on the ratio between local surface orientations over the whole irradiated area.

TABLE I. In this table are reported the parameters used to simulate both the phase scan and emission curves.

a_1 [cm^2 A^{-1}]	$(2.5 \pm 0.1) \times 10^{-14}$
a_2 [cm^4 A^{-2}]	$(7.0 \pm 0.1) \times 10^{-25}$
β_{ph}	1.5 ± 0.1
φ [eV]	4.60 ± 0.2

It should not be surprising the fact that, even if the surface work function obtained from the best fit of the emission curve has a value lower than the energy of UV photons, the emission curve shows a quadratic behavior. The non-negligible contribution of a two-photon emission may be ascribed also to the high laser power density delivered to the cathode by the 35 fs rms long laser pulses. Using the same a_1, a_2, β_{ph}, and φ of Table I, we calculated the charge extracted as a function of the launch phase for the case of a 10 ps FWHM long laser pulse, with the same transverse profile and the same energy per pulse. The fraction of the emitted electron charge that can be ascribed to the two-photon emission process would decrease more than 2 orders of magnitude for such long laser pulses with respect to our experimental results. It is possible to deduce from the $a1$ coefficient the quantum efficiency for the one-photon emission process of about 1.2×10^{-5}. The $a2$ coefficient deduced value is similar to that obtained for other metals [13].

B. Dark current

The charge collected by the FC was measured using a noise filter and an oscilloscope. The dark current pulse duration was 1.5 μs. The macropulse structure is given by a train of micropulses centered in time on the peaks of the rf wave [14] and was measured integrating all the peak contributions over the rf macropulse duration resulting in average current values on the order of few μA. The following modified Fowler-Nordheim formula for a sinusoidally varying electric field can be used to model the field emission of the cathode:

$$I_{\mathrm{FN}} = \frac{5.7 \times 10^{-12+4.52\phi^{-0.5}} A_e (\beta_{\mathrm{FE}} E_0)^{2.5}}{\phi^{1.75}} \times \exp\left(-\frac{6.53 \times 10^9 \phi^{1.5}}{\beta_{\mathrm{FE}} E_0}\right), \quad (5)$$

where E_0 is the sinusoidal amplitude of the surface field expressed V/m, β_{FE} is the enhancement factor for the electron field emission process, φ is work function expressed in eV, and A_e is the effective emitting area expressed in m^2 [15].

The solenoid field was set at 1.3 kGs, to maximize the collected charge measured by the FC. We observed experimentally that it was not necessary to change the focusing strength of the solenoid to collect all the charge in the FC

within the range of electric field used, mostly due to the large acceptance area of the FC (3 cm diameter).

In order to extract information from this measurement, our analysis proceeds as follows. First, we assume that the main contribution to the current comes from the cathode area, and the electrons emitted from other surfaces in the gun do not reach the FC [14]. We then rescale the experimental data in the form of a Fowler-Nordheim plot, obtaining the graph reported in Fig. 6.

Fowler-Nordheim theory states a linear relationship between the inverse of electric field amplitude and the logarithm of the ratio between the average current and the intensity of the electric field raised to 2.5 power [16]. It can be seen that for larger field values reported in Fig. 6 the curve becomes linear as expected. The ''shoulder'' of the plot for lower electric field values is probably due to an intermediate regime in which different cathode areas start to emit a sizable current for different field levels, according to their local geometric enhancement factor. Above this threshold, which in our case was at about 50 MV/m, the emission area becomes constant, and the cathode emission finally obeys the Fowler-Nordheim theory. More detailed studies are foreseen to elucidate the unexpected shoulder observed for lower electric field values. In particular, we are trying to develop a numerical model that will take into account the density of states of Mg and the real temperature of the metallic cathode surface. Only the part of the curve above the threshold will be considered in the following discussion.

A linear fit of a Fowler plot gives the values of the field enhancement factor and the emission area. A final assumption on the work function of the cathode is necessary. Using the value of $\varphi = 4.6$ eV determined with photoemission measurements described in the previous paragraph, we calculate an enhancement factor $\beta_{\mathrm{FE}} \sim 120$ and an effective emitting area of about $A_E \times 10^{-14}$ m^2. Both these values are consistent with values measured on metallic surfaces by other groups [15].

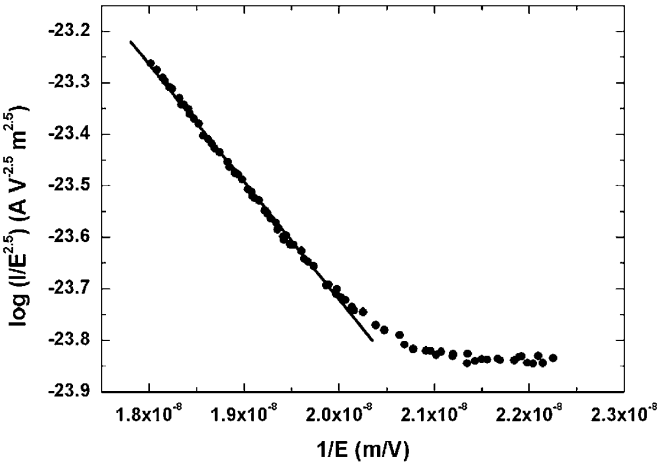

FIG. 6. Dark current measurements: in this Fowler-Nordheim plot are reported the experimental data and the linear best fit from which the β_{FE} and A_e coefficients are deduced.

C. Thermal emittance

An important quantity related to the photocathode performance in terms of e-beam quality is the thermal emittance. When the electrons are emitted from the photocathode, they have an angular spread which depends on the excess kinetic energy E_k arising from the difference between the energy of the driver laser photon energy and the cathode work function. The thermal emittance is proportional to this angular spread and to the laser spot size sigma_l. In other words the beam rms emittance is given by [17]

$$\varepsilon_{nx} = \sigma_{x\_\mathrm{laser}} \sqrt{\frac{E_k}{mc^2}}. \tag{6}$$

To measure this quantity, we used the technique proposed by Graves [18] utilizing a fluorescent screen intercepting the beam downstream the gun/solenoid assembly. Electron rms size is measured on the screen for different focusing strengths of the solenoid. It is evident from (6) that the measured emittance will show a linear dependence on the rms spot size of the laser. A linear fit of the measured emittance values obtained for different laser spot sizes yields the rms spread in emission angles intrinsic of the cathode.

To analyze the data, we model the focusing effect of the solenoid as a thick lens matrix. Electron beam size at the screen (subscript 1) as a function of starting position and momentum (subscript 0) can be written as

$$\langle x_1^2 \rangle = R_{11}^2 \langle x_0^2 \rangle + 2R_{11}R_{12}\langle x_0 x'_0 \rangle + R_{12}^2 \langle x'^2_0 \rangle \tag{7}$$

with $\boldsymbol{R}_{ij}$ being the solenoid matrix elements and the quantities in the angled square the beam second order moments. A fitting on the experimental data yields second order moments retrieval, and hence, to the emittance, according to

$$\varepsilon_{nx} = \beta\gamma \sqrt{\langle x_0^2 \rangle \langle x'^2_0 \rangle - \langle x_0 x'_0 \rangle^2}. \tag{8}$$

In order to be consistent with (7), linear transport of the beam must be ensured. Space charge and rf contributions must be negligible in order to avoid systematic errors on the emittance value. Space charge is minimized by using a very low charge of 2 pC for the measurements. The rf contribution is related to the bunch extent in the rf wave and was also minimized using a very short laser pulse length (less than one-tenth of a degree of rf wave).

The transverse emittances (both horizontal and vertical) measured for different spot sizes are reported in Fig. 7. Measurements yielded 0.85 and 0.75 mm mrad for 1 mm rms spot radius, respectively, for horizontal and vertical emittance. A similar value of emittance has been measured for Cu cathodes (0.93 mm mrad for 1 mm spot radius) [18].

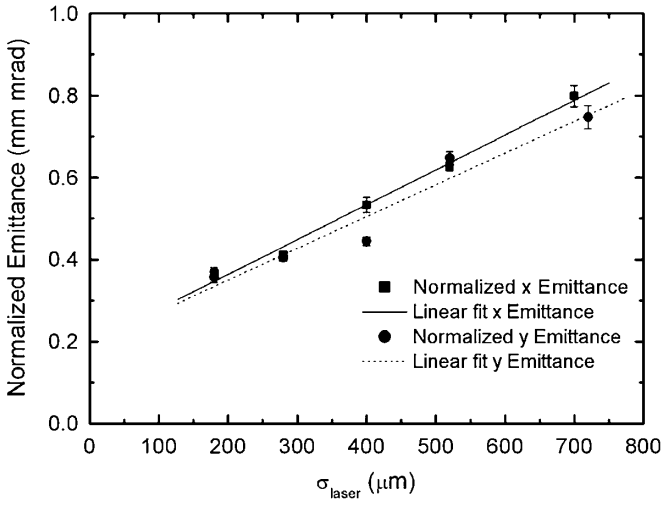

FIG. 7. Linear relationship between normalized emittance and laser distribution standard deviation: experimental data and best fit.

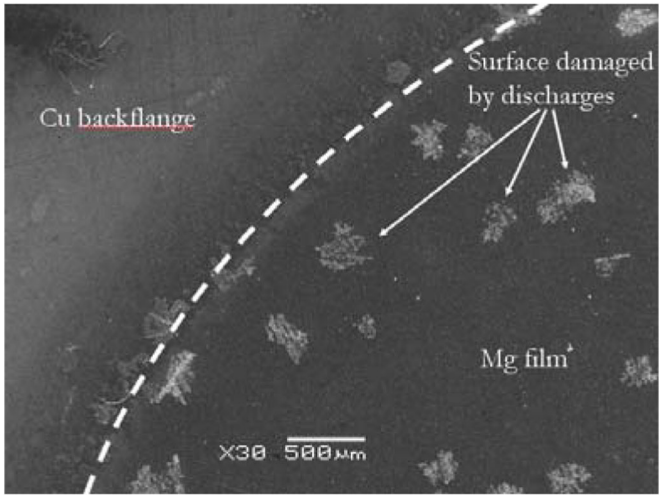

FIG. 8. SEM micrograph of the Mg film over the Cu backflange after the removal from the rf gun: the white dashed line evidences the border of the Mg film. Several damaged areas are also clearly evident.

As discussed before, the work function value of 4.6 eV deduced from our dark current and photoemission measurement is consistent with an amorphous MgO layer on the cathode surface and quite similar to Cu work function justifying similar values of thermal emittance of Cu and our Mg sample surface, and showing that the emittance is not increased by any spurious factor such as film morphology or surface roughness.

D. Surface characterization (SEM and EDX)

After a few months of operation, the backflange with the Mg thin film cathode has been removed from the gun and surface analyses have been performed by means of SEM and EDX techniques.

Figure 8 reports a picture of an area of the Cu backflange where also is visible a portion of the surface covered by Mg film. The dashed line indicates the circular boundary of the Mg film. It is evident that the surface of the Mg film has been damaged in several points by electrical discharge generated during rf-gun conditioning and operation, as expected. These damaged spots appear to be uniformly distributed over the whole film surface with sizes of a few hundreds of microns. In order to quantify the damage level caused by such discharges, one of these spots was analyzed by means of EDX with the aim to obtain a compositional map of the surface.

The maps obtained by SEM-EDX are reported in Fig. 9. They have been obtained with 5 keV electrons in order to decrease the contribution of the x rays coming from the Cu substrate. In these experimental conditions, no signal of Cu substrate has been detected inside the observed area: the box relative to the Cu EDX map in Fig. 9 appears black because no x rays coming from the substrate have been detected. The maps reveal that electric discharge, even if the surface appears clearly damaged, has not removed the Mg film from the Cu substrate. The map of Mg does not seem to present evident voids or craters; it means that the film has not been completely removed from the surface. The oxygen map shows a higher concentration of this element in the damaged area. The reasons for this effect are at this moment not yet well understood: a role can be played by the increase of local temperature in the discharge area promoting the local reactivity of Mg towards oxygen containing chemical species; moreover, the Mg clean surface generated by discharges may have increased the oxidation process rate when the flange was removed from the gun. Anyway, only with new dedicated experiments will it be possible to understand the reasons for these different

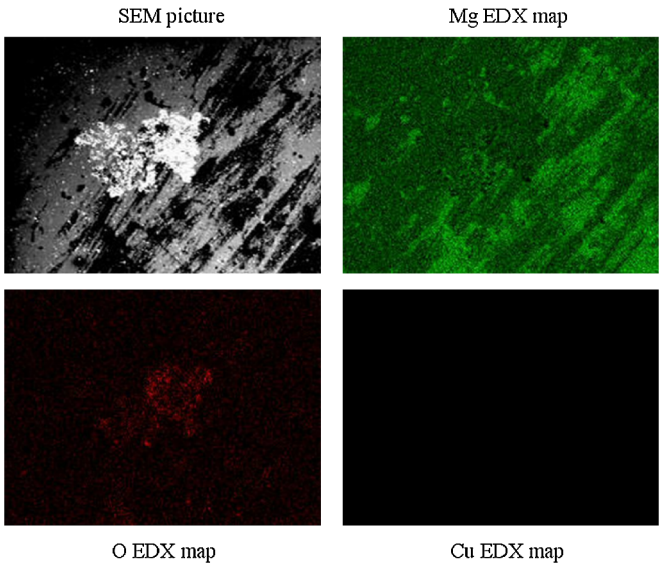

FIG. 9. EDX maps of the Mg film surrounding a clearly visible damaged area.

oxidation rates. The most important information that we can deduce from surface characterizations is that the Mg film deposited by PLD over the Cu backflange has not been removed during the conditioning and normal operation of the rf gun. Moreover, electric discharges did not pierce the film and expose the Cu substrate to the drive laser radiation, as evidenced by the total absence of a Cu signal in EDX maps. It is important to note here that this film was not optimized from the point of view of the thickness. The tested Mg film was only 500 nm thin, while the PLD technique can deposit Mg coating with thickness of some micron [6], enough to ensure higher protection towards the piercing induced by electrical discharge.

IV. CONCLUSIONS

In this article we report the results of the first power tests of a PLD deposited film used as a photocathode in an rf gun. The film on the backflange was oxidized during transport and installation and has undergone the usual conditioning process. The electric field gradient in the gun has been brought up to 100 MV/m. During this phase, unavoidable discharges took place and were uniformly distributed on the film surface. SEM and EDX analyses indicate that such discharges have partially damaged the film without exposing the Cu substrate, notwithstanding its small thickness (~ 500 nm). No laser cleaning procedure was performed, due to insufficient laser energy density. After conditioning, the gun was operated for several months in experiments where the cathode was illuminated by very short (50 fs) intense (10 μJ) laser pulses to demonstrate a novel regime of operation of rf photoinjector dominated by space charge expansion [19]. In those experimental conditions the photoelectron emission was originated mainly by two-photon processes, according to our experimental data and numerical simulation. This could have caused an even larger cathode emittance in those experiments than the one measured here. The thermal emittance measurements discussed in this paper were conducted with very low charge in order to avoid nonlinearities. The measured value therefore refers to the single photon process. The measured thermal emittance was about 1 mm mrad for 1 mm rms spot radius, similar to that of nonideal Cu. This is explained by the similar values of the work functions of Cu and our Mg film, and suggests that the emittance is not further degraded by film morphology.

A moderate value of the field enhancement factor (~ 1.5) has been deduced by fitting to an experimental phase-scan curve. The measured dark current level (some μA) averaged over the rf pulse is also similar to that of normal Cu cathodes [15].

More power tests are needed on thicker films (few microns) and with laser cleaning to study the emission properties of pure Mg-based photocathodes.

ACKNOWLEDGMENTS

This work was supported by Italian National Institute of Nuclear Physics (INFN) and by Ministero Istruzione Università e Ricerca, Progetti Strategici, DD 1834, December 4, 2002. The work at the UCLA Pegasus laboratory was partially supported by ONR Grant No. N000140711174.

[1] C. Pellegrini, in *Proceedings of the European Particle Accelerator Conference, Stockholm, Sweden, 1998* (IOP Publishing, Bristol, UK, 1998).

[2] H. H. Braun, E. Chevallay, S. Hutchins, P. Legros, G. Suberlucq, H. Trautner, I. N. Ross, and E. Bente, in *Proceedings of the Particle Accelerator Conference, Chicago, IL, 2001* (IEEE, Piscataway, NJ, 2001).

[3] T. Srinivasan-Rao, J. Fischer, and T. Tsang, J. Appl. Phys. **69**, 3291 (1991).

[4] T. Srinivasan-Rao, J. Schill, I. Ben-Zvi, and M. Woodle, Rev. Sci. Instrum. **69**, 2292 (1998).

[5] X. J. Wang, M. Babzien, I. Ben-Zvi, R. Malone, J. Sheehan, J. Skaritka, T. Srinivasan-Rao, M. Woodle, V. Yakimenko, and L. H. Yu, in *Proceedings of 19th International Linear Accelerator Conference, Chicago, IL* (Argonne National Laboratory, Argonne, Illinois, 1998), p. 886.

[6] L. Cultrera, C. Ristoscu, G. Gatti, P. Miglietta, F. Tazzioli, and A. Perrone, J. Phys. D **40**, 5965 (2007).

[7] L. Cultrera, G. Gatti, P. Miglietta, F. Tazzioli, and A. Perrone, Nucl. Instrum. Methods Phys. Res., Sect. A **587**, 7 (2008).

[8] D. T. Palmer, R. H. Miller, H. Winick, X. J. Wang, K. Batchelor, M. Woodle, and I. Ben-Zvi, in *Proceedings of the Particle Accelerator Conference, Dallas, TX, 1995* (IEEE, Piscataway, NJ, 1995).

[9] G. Gatti, F. Tazzioli, C. Vicario, I. Boscolo, S. Cialdi, L. Cultrera, A. Perrone, M. Rossi, S. Orlanducci, and M. L. Terranova, in *Proceedings of the Particle Accelerator Conference, Knoxville, TN, 2005* (IEEE, Piscataway, NJ, 2007).

[10] G. Gatti, L. Cultrera, F. Tazzioli, A. Perrone, P. Musumeci, and J. Moody, in *Proceedings of the Particle Accelerator Conference, Albuquerque, NM, 2007* (IEEE, Piscataway, NJ, 2007).

[11] P. Musumeci, J. Moody, and G. Gatti, in Proceedings of the Particle Accelerator Conference, Albuquerque, NM, 2007 (Ref. [10]).

[12] L. A. Dubridge, Phys. Rev. **39**, 108 (1932).

[13] J. H. Bechtel, W. L. Smith, and N. Bloembergen, Phys. Rev. B **15**, 4557 (1977).

[14] I. Bohnet, J. H. Han, M. Krasilnikov, F. Stephan, and K. Flöttmann, in *Proceedings of the 6th European Workshop on Beam Diagnostics and Instrumentation for Particle Accelerators, Mainz, Germany, 2003* (GSI, Darmstadt, Germany, 2003).

[15] J. W. Wang and G. A. Loew, SLAC Report No. SLAC-PUB-7684, 1997.

[16] R. H. Fowler and L. Nordheim, in Proc. R. Soc. London **119**, 173 (1928).
[17] J. D. Lawson, *The Physics of Charged Particle Beams* (Oxford University Press, Oxford, England, 1988).
[18] W. S. Graves, L. F. DiMauro, R. Heese, E. D. Johnson, J. Rose, J. Rudati, T. Shaftan, and B. Sheehy, in Proceedings of the Particle Accelerator Conference, Chicago, IL, 2001 (Ref. [2]).
[19] P. Musumeci, J. T. Moody, R. J. England, J. B. Rosenzweig, and T. Tran, Phys. Rev. Lett. **100**, 244801 (2008).